Journal of Solid State Chemistry **146,** 516–527 (1999)
Article ID jssc.1999.8373, available online at http://www.idealibrary.com on IDEAL®

Photographic Sensitization of the AgBr(100) Surface and the Effect of Au and S in Latent Image Formation: A Detailed Theoretical Mechanism

Abds-Sami Malik,* John T. Blair,† William A. Bernett,‡,[1]
Francis J. DiSalvo,* and Roald Hoffmann*,[2]

*Department of Chemistry, Cornell University, Ithaca, New York 14853; †Imation Corporation, Oakdale, Minnesota 55128; and ‡3M Company, St. Paul, Minnesota 55144

Received October 20, 1998; in revised form April 26, 1999; accepted May 10, 1999

Recent experimental characterization of the Au-doped reconstructed AgBr(111) surface has been used to construct a theoretical model (using an approximate molecular orbital method) of that surface. The surface consists of a half-layer covering of Ag segregated into rows 7.07 Å apart, with the Au in interstitial sites just below the surface. Our calculations indicate that the surface Ag *s*-orbital form states at the bottom of the conduction band, which could serve as trapping sites for photoelectrons. The gold atoms do not contribute directly to these states. We also construct models (based on experimental data) of the AgBr(100) surface with ledge and kink type point defects and of an AgBr(111) : Ag_2S(100) interface. The theoretical models provide a mechanism for the formation of a latent subimage through trapping of photoelectrons and subsequent pairwise distortion of the surface Ag. This model predicts that latent subimage formation is more favorable on AgBr(111) surfaces than on AgBr(100) surfaces and that Au contributes to the stability of a latent subimage cluster. Calculations of an AgBr(111) : Ag_2S(100) interface show that interface formation leads to a smaller band-gap. The formation of a latent subimage cluster is thus facilitated.

Silver halides have been the basis of photography for over 150 years. In modern photographic film, the light sensitive surface consists of an emulsion of AgBr (which has the NaCl structure type) microcrystals of octahedral and tabular (presenting the (111) surface) or cubic (presenting the (100) surface) morphologies. The former is found in most commercial preparations and is empirically known to possess greater photographic sensitivity than the latter (1). Gold and sulfur dopants are also added to further improve photographic sensitivity (1). Experimental evidence shows that silver sulfide, silver gold sulfide, and Au^0 are formed during this process (2–4), although there is still controversy regarding the presence of Au^0 (4).

Despite great advances in film quality and sensitivity, a sound theoretical framework describing the elementary acts of the photographic process at the atomic level has been taking shape much more slowly. In a previous paper, we used an approximate molecular orbital method to explore the mechanism of latent image formation on the reconstructed (111) surface of AgBr (5). In this contribution, we extend our analysis to the AgBr(100) surface and also investigate the role of sulfur and of gold sensitization on latent image formation.

Calculations were done of an AgBr(111) reconstructed surface with Au dopant of an AgBr(100) surface with point defects and of an AgBr(111) : Ag_2S(100) interface. The extended Hückel method (6) was used for all band structure calculations. This is an approximate molecular orbital method with well-recognized limitations. While it does not predict absolute energies reliably, it does capture the general bonding characteristics of a wide range of discrete and extended structures. In particular, it is able to describe the electronic structure of AgBr surfaces and of an AgBr : Ag_2S interface in some detail. The method and the parameters are described in the Appendix, as are details of the geometry used.

In our analysis, we invoke some of the ideas of photoelectrons and trapping sites first expounded by Gurney and Mott (7). Theoretical densities of states (DOS) (6d) and crystal orbital overlap population (COOP) (6b) curves are central to our discussion. Throughout this paper we use Ag and Br as symbols for atom types, without any implication as to the specific ionicity of these centers.[3]

[1] Former affiliation.
[2] To whom correspondence should be addressed.

[3] They, in fact, emerge carrying not much charge in our calculations. The ionicity is greater toward the surface than in the bulk. Please see Ref. (5) for details.

0022-4596/99 $30.00

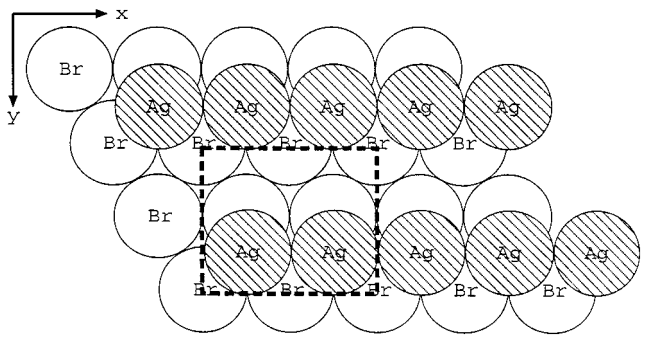

FIG. 1. A view of the AgBr(111) reconstructed surface. The surface silver half layer segregates into rows that are 7.07 Å apart. The Ag–Ag distance within the rows is 4.08 Å. The unit cell that was used in the calculations is outlined by a dashed line.

CALCULATIONS

The AgBr(111) Surface and Bulk AgBr

Although we have previously reported our findings about the (111) surface (5), it seems appropriate to briefly summarize those results here, in order to compare it with the (100) surface.

Since AgBr crystallizes in the rocksalt structure type, an ideal (111) surface presents a layer of either bromine or silver ions. However, this ideal surface undergoes reconstruction (8–11) to give a half-layer covering of silver ions arranged in rows (12, 13), as shown in Fig. 1. We constructed a theoretical model of this surface and found that its DOS (Fig. 2b) manifests a peak at the bottom of the conduction band. The DOS of bulk AgBr (Fig. 2a) shows that our calculated band gap of 2.5 eV reasonably reproduces the experimental result that AgBr is a wide band-gap, indirect gap semiconductor (14). As shown in the figures, this peak is mainly due to surface Ag *s*-states. It was identified as a shallow trapping site for photoelectrons (5, 6c).

We then provided a mechanism, through a Peierls distortion, which involved the pairing of Ag atoms on the surface (6d), for the formation of a primitive two-atom 'latent subimage cluster' (1a) on the reconstructed AgBr(111) surface. The peak in the DOS moves down in energy (Fig. 2c) as the atoms move pairwise toward each other, suggesting that this distortion is energetically favorable if some photoelectrons are present. For further details, the reader is directed to our recent paper (5).

The AgBr(100) Surface: Kink Defect

The (100) surface, unlike the (111) surface, has not been found to undergo reconstruction (13). However, ledge or kink type defects can be formed on the surface (15). These point defects have been the subject of several investigations in latent image formation (16–18). It has been postulated

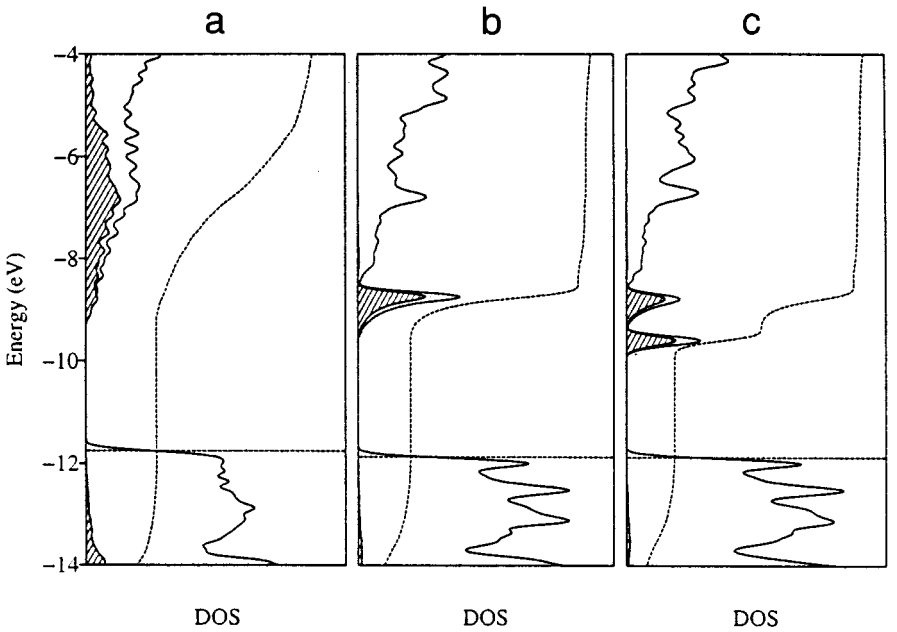

FIG. 2. The following conventions apply for all DOS curves in this paper: the horizontal dashed line is the Fermi level, the solid line is the total DOS, the shaded region denotes the specified contribution to the total DOS, and the dotted curve is the integration of that specified contribution. The leftmost panel shows the DOS of bulk AgBr. The middle panel shows the DOS of the (111) reconstructed surface model. The rightmost panel shows the DOS of the (111) surface after the pairing distortion. (a) Solid AgBr : Ag *s*-orbital. (b) AgBr surface : surface Ag *s*-orbital, Ag–Ag 4.08 Å. (c) AgBr surface : surface Ag *s*-orbital Ag–Ag 3.10 Å.

that these sites are places where a latent image cluster could preferentially form.

A six-layer slab model (including one defect layer) of the AgBr(100) surface was constructed to investigate the electronic properties of these ledge and kink defect sites. Figure 3 shows the model used for the kink defect. Note that the Ag's are at the protruding corners of the kink. The local coordination environment of the corner Ag is similar to that found on the (111) reconstructed surface (Fig. 1) in that the corner Ag has only three nearest neighbor Br atoms. Because of this, it is reasonable to expect that some motion of the corner Ag would be facile, if there be an electronic reason for it.

The unit cell that was used in the calculations is also shown in Fig. 3. There are two corner Ag's per unit cell. The cell was chosen to be large enough to approximate the local environment of the corner Ag to the nearest and next-nearest neighbors.

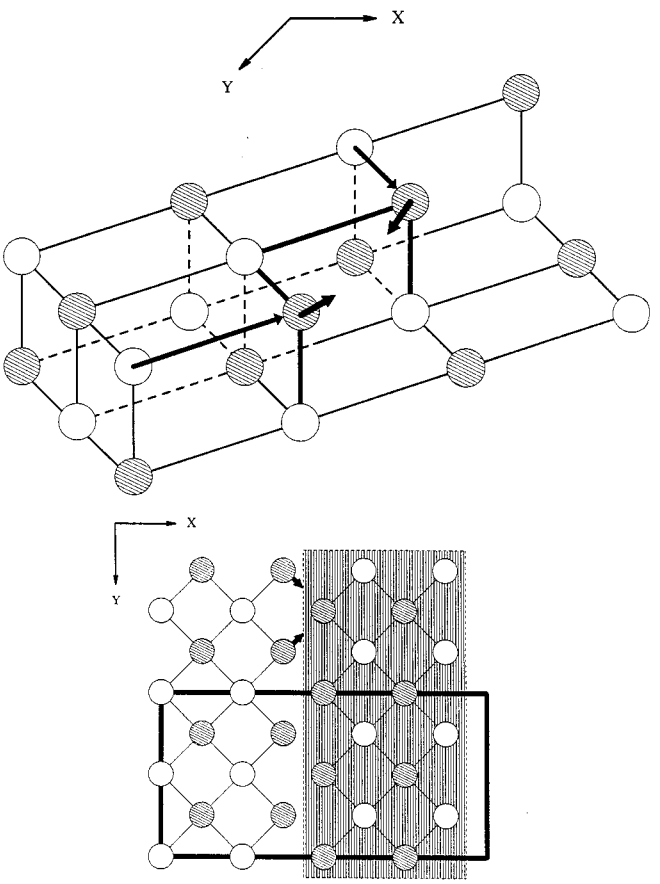

FIG. 3. Two views of a kink defect are shown. The top figure shows a kink defect in perspective while the bottom figure shows the defect from the top. The shaded spheres are Ag while the unshaded ones are Br. The distortion described in the text is indicated by the arrows. Two Ag's at the corners move toward each other while the Ag–Br distances marked by heavy lines (in the top figure) are kept constant. The Ag–Br distance that is marked by a heavy line with an arrow is allowed to stretch. The motion can be described as two hinges closing. In the bottom figure, the portion that is shaded and outlined by a dashed line is one layer below the unshaded portion. The box marked by a heavy line represents the unit cell that was used in the calculations.

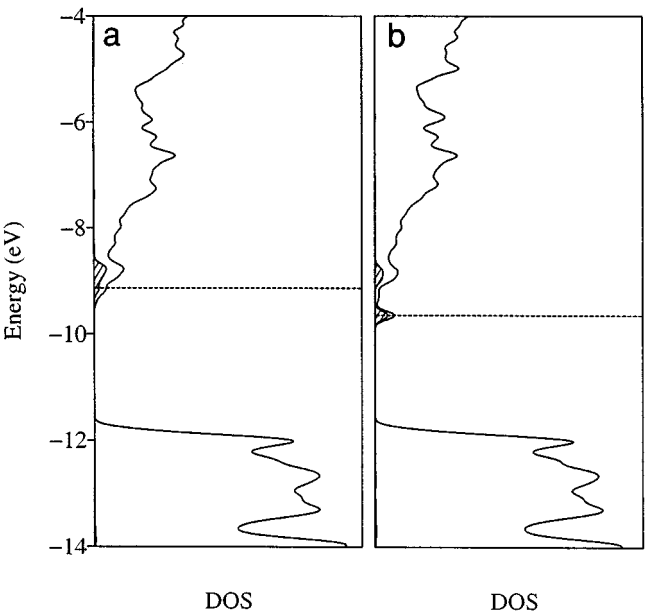

FIG. 4. The DOS of the AgBr(100) slab model with a kink defect. The Fermi level has been indicated for one extra electron per pair of Ag at the kink site. The DOS contribution from Ag *s*-states at the kink is shown in projection. The left and right panels show the DOS before and after the deformation described in the text and Fig. 3 takes place. (a) Ag–Ag 4.08 Å and (b) Ag–Ag 3.10 Å.

Figure 4a shows the DOS of AgBr(100) with a kink defect. We see again a peak at the bottom of the conduction band similar to the one that was observed in the case of the (111) surface. Now, however, the peak is not as pronounced as was observed previously. The projected DOS shows only the contribution to this peak from the Ag *s*-states at the kink defect; other surface Ag *s*-states (not at the kink) also contribute. The question naturally arises as to whether this peak can also serve as a shallow trap for photoelectrons. The Fermi level in Fig. 4 is indicated for one electron extra per pair of Ag's at the kink site, showing that these states can indeed serve as shallow traps for photoelectrons.

We postulate a pairing distortion of two Ag's at the kink, analogous to what we described previously (5). This distortion is indicated with arrows in Fig. 3; it involves the motion of two Ag atoms at a kink defect toward each other, while keeping most of the Ag–Br distances constant. At the beginning of the distortion, the Ag–Ag distance is 4.08 Å; at the end of the distortion, it is 3.10 Å.

The resulting DOS after the distortion has occurred is shown in Fig. 4b. Some of the states near the bottom of the conduction band have moved down in energy, clearly indicating that there has been energy stabilization corresponding to the distortion. This is reminiscent of the situation shown

earlier in Fig. 2. This stabilization, however, is not as great as had been observed for the (111) case.

The AgBr(100) Surface: Ledge Defect

Ledge defects can also form on a (100) surface. Using the same approach as described in the previous section, a calculational model (Fig. 5) of such a defect was constructed. Note that the Ag at the ledge edge has four near-neighbor Br atoms, more than Ag at a kink defect (Fig. 3) or Ag on a (111) surface (Fig. 1). This observation suggests that it will be more difficult to distort the Ag.

The DOS of AgBr(100) with a ledge defect is shown in Fig. 6a. The Fermi level has been indicated for a neutral slab. Unlike the DOS of either the (100) surface with kink defects (Fig. 5) or the (111) surface (Fig. 2), there is not a dramatic peak at the bottom of the conduction band. The ledge defect also does not display a localization of Ag *s*-states from the Ag at the ledge edge. We cannot identify a shallow trap for photoelectrons in this case.

However, there is a plausible distortion involving the Ag at the ledge. This distortion is indicated with arrows in Fig. 5. An Ag at the ledge moves in an arc directly toward an Ag on the lower level. The proposed distortion does not involve the motion of two atoms. Only the Ag at the ledge is moved, as indicated by the arrows. Nevertheless, this distortion can still be considered a pairing distortion in that it involves the interaction of two Ag, now on different layers of the surface. The Ag–Ag distance is taken to move from 4.08 Å at the beginning of the distortion to 3.10 Å at the end.

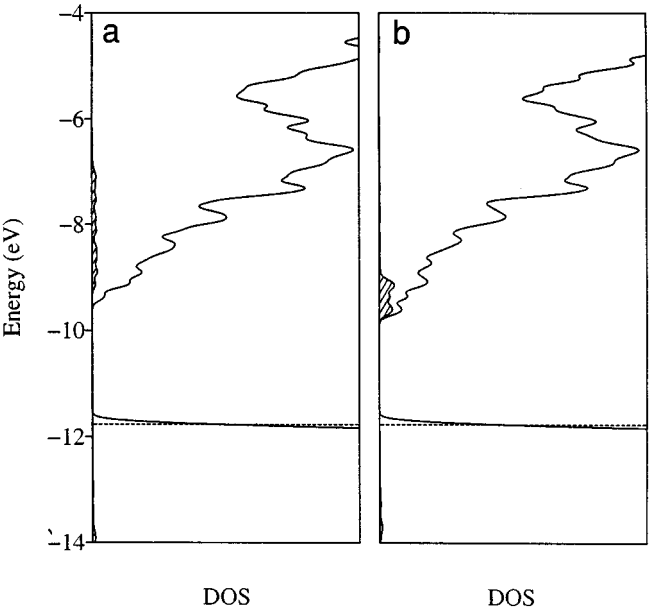

FIG. 6. The DOS of the AgBr(100) slab model with a ledge defect. The Fermi level has been indicated for a neutral slab. The DOS contribution from Ag *s*-states at the ledge is shown in projection. The left and right panels show the DOS before and after (respectively) the deformation takes place. (a) Ag–Ag 4.08 Å and (b) Ag–Ag 3.10 Å.

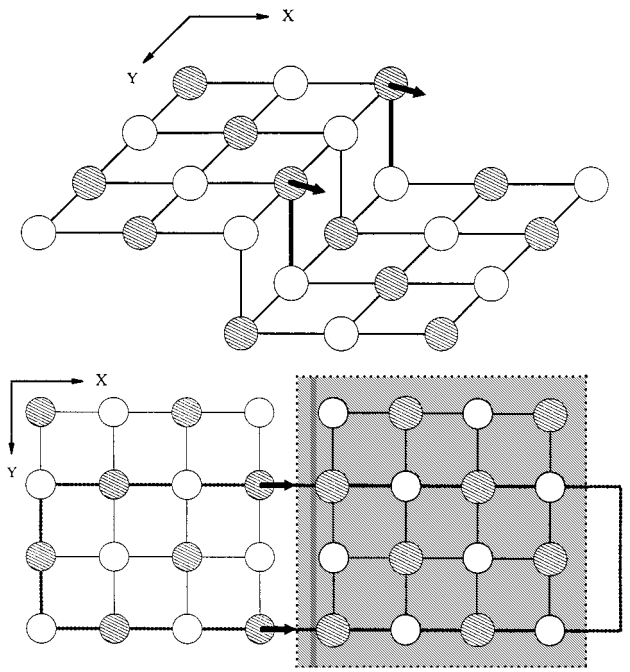

FIG. 5. Two views of a ledge defect are shown. The top figure shows a perspective view while the bottom figure shows the same from the top. The shaded spheres are Ag while the unshaded ones are Br. The distortion described in the text is indicated by the arrows. An Ag at the ledge is postulated to swing in an arc toward an Ag in the next lower plane. Only Ag at the ledge is moved. The Ag–Br distance marked by a heavy line (in the top figure) is kept constant. In the bottom figure, the portion that is shaded and outlined by a dashed line is one layer below the unshaded portion. The box marked by a heavy line represents the unit cell that was used in the calculations.

The resulting DOS for this distortion is shown in Fig. 6b. The Ag *s*-states at the ledge become localized near the bottom of the conduction band in this distortion. The bottom of the conduction band has moved slightly down in energy, so there is some stabilization that results from the distortion, but not much. This distortion is clearly the least favorable of the ones considered so far.

The Effect of an Au Interstitial

In the introduction, we mentioned that Au impurities are intentionally added to enhance photographic sensitivity. The reason for this enhancement is not clear, though it has been postulated that the presence of Au facilitates the formation of a latent image cluster (19, 20). It is argued that Au^0 increases fog (and is thus undesirable), whereas if gold is present as Au^+, photographic sensitivity is enhanced (21). However, there has been some disagreement on this point (4). Experimental evidence shows that both oxidation states of Au are present in commercial preparations (2, 3).

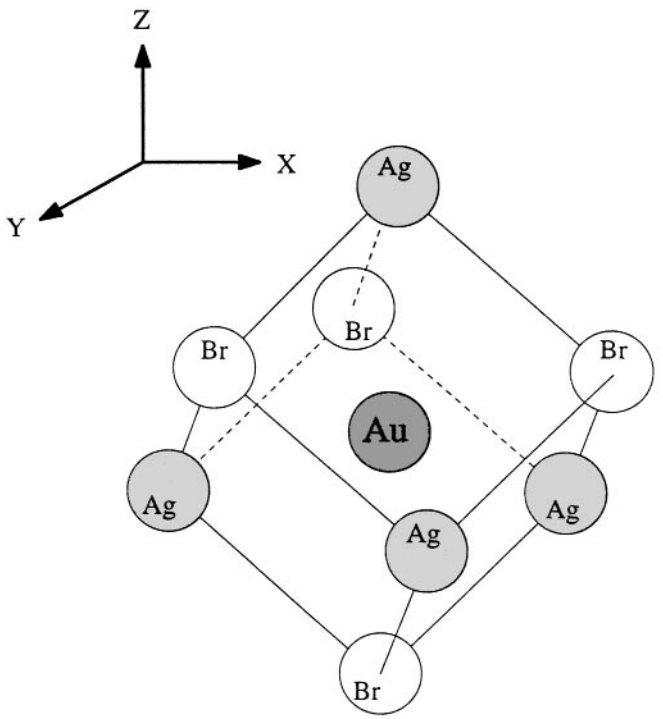

FIG. 7. The local geometry of interstitial Au near the AgBr(111) surface is shown. The uppermost Ag in the figure is one of the surface Ag shown in Fig. 1. The interstitial Au is directly below this surface Ag.

Very recently, a preliminary SEXAFS study was done of Au on AgBr surfaces (26) in which the investigators describe an "interstitial" site for adsorbed Au on the reconstructed AgBr(111) surface. We used this experimental data to construct a theoretical model to study the effect of Au^0 on latent image formation.

Figure 7 shows the local coordination of this adsorbed Au. Each Au sits just below a surface Ag (please see Fig. 1) and is tetrahedrally coordinated by one surface and three inner Ag's. It also has four Br neighbors. An alternative description is that the Au is in the middle of a "cubane" cluster formed by Ag and Br.

In the calculations, one neutral Au interstitial for every two surface Ag's was introduced.[4] Figure 8 shows the DOS of the AgBr(111) surface with the contribution of the Au interstitial to that DOS. The DOS is not substantially different from the one shown in Fig. 2b. There are no new states in the band-gap region, and, more importantly, there is no contribution from the Au to the DOS in this region. However, the surface Ag *s*-band is populated by electron transfer from the neutral Au, as shown by the location of the Fermi level. Essentially, Au atoms are oxidized, releasing their electrons into the AgBr conduction band. The net effect is that one electron per two surface Ag's has been transferred to the surface Ag *s*-band. If the surface Ag is considered to be carrying (formally) a +1 charge, then only one more electron (in addition to the one donated by the Au interstitial) per two surface Ag's is required to complete the reduction of all surface Ag ions to neutral Ag.

The presence of Au essentially sensitizes the surface so that fewer photoelectrons are needed in the formation of a latent subimage center. The same driving force for Ag–Ag pairing as was analyzed in the case of AgBr(111) surfaces (5), albeit weaker if there are no photoelectrons, is created upon the addition of Au. If photoelectrons are present, the tendency to pair will be greater.

Energetics and Bond Formation for Reduced AgBr Surfaces

In order to gauge the stabilization upon Ag–Ag surface pairing and the corresponding growth in strength of some surface Ag–Ag bonds, calculations were done as described previously, varying incrementally the Ag–Ag distances involved in the distortion from 4.08 to 3.10 Å. The following calculations were done: (a) the AgBr(100) surface with kink defect, (b) the AgBr(100) surface with ledge defect, and (c) the

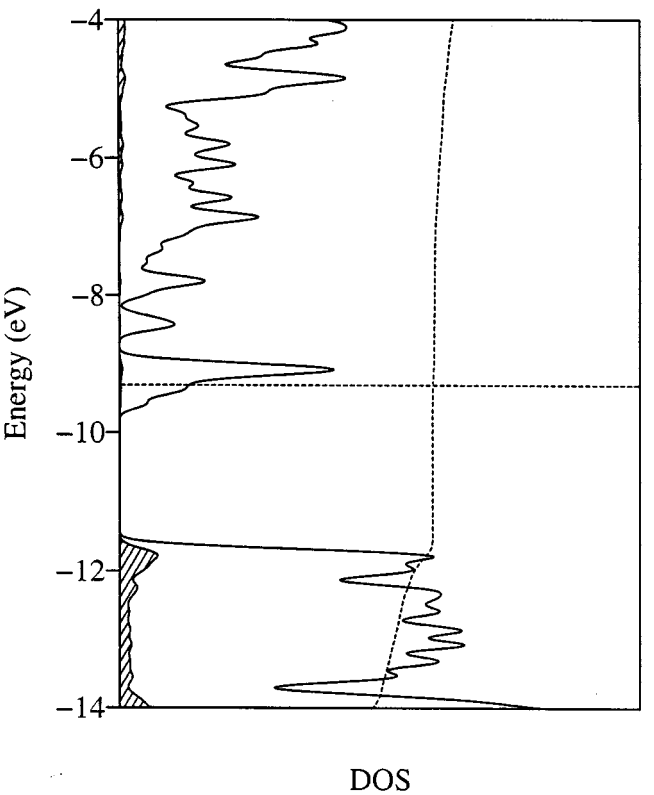

FIG. 8. The DOS of the AgBr(111) slab model with Au interstitial (one Au per two Ag surface atoms) is shown. The contribution of Au to the DOS and the Fermi level is indicated. Note that the important DOS peak at −9.10 eV is essentially unaffected.

[4]The same unit cell as shown in Fig. 1 was used, with the addition of interstitial gold.

AgBr(111) reconstructed surface with an Au interstitial. In each of the surface models, calculations were also done with varying electron counts corresponding to the potential number of photoelectrons (up to a total of two) per pair of Ag involved in the distortion. For calculation (c), only up to one photoelectron per pair of Ag was considered, for the reasons given in the previous section. Thus for each calculation, there were three cases studied (0, 1, and 2 photoelectrons per pair of Ag's); except in the calculation with gold, in which two cases were studied (0 and 1 photoelectrons per pair of Ag's). The relative stabilization energies and overlap populations (OP) were calculated for each model.

In order to measure the extent of Ag–Ag bonding, it is important to have a model for such bonding. Two neutral Ag atoms should give a model of an Ag–Ag single bond; and two Ag^+ ions should interact only weakly. As a calibration, the following calculations were done for diatomic molecules, specifically: (d) two Ag^+ ions interacting, (e) one Ag^0 and one Ag^+ interacting, and (f) two Ag^0 interacting. The OP and net energy stabilization for each case were calculated. These results have been summarized (for overlap population) in Fig. 9 and (for energy stabilization) in Fig. 10. For clarity, each set of calculations is summarized in separate plots with the calculations for diatomics included in each plot.

The reference system of Ag^+–Ag^+, which one might expect to be repulsive (d^{10}–d^{10}), is actually slightly attractive (in energy) and bonding (judged by the OP). The reason for this phenomenon has been discussed for Cu^+–Cu^+. It has been suggested that it is due to *s*, *p* orbital mixing into the *d* block (23, 24). Other explanations for such d^{10}–d^{10} attractions in coinage metals have been proposed (25).

For these model diatomics, the overlap population and relative energy stabilization indeed increase as one goes from Ag^+–Ag^+ to Ag^0–Ag^+ and are greatest for two Ag^0 interacting. Turning to the surface calculations, as far as the OPs are concerned, this trend is reflected for two surface silvers pairing in all three of the models studied. Figure 9 shows that the overlap population is greater for two electrons per two Ag's than for one electron per two Ag's and is lowest for no electrons per two Ag's. With the inclusion of an Au interstitial, the overlap population is greater for one Au and one electron per two Ag's than for one Au and no electron per two Ag's. The OP values with Au included are essentially what would be expected if the Au is considered to be simply transferring electrons to the surface Ag. The general trend is followed for the relative stabilization energy, as shown in Fig. 10. For the (100) surfaces, there seems to be no stabilization energy to be gained from deformation at the defect, although the inclusion of one or two electrons makes the distortion successively more favorable. Also note that the deformation at a kink site is more favorable. In the (111) surface with Au, there is greater energy stabilization

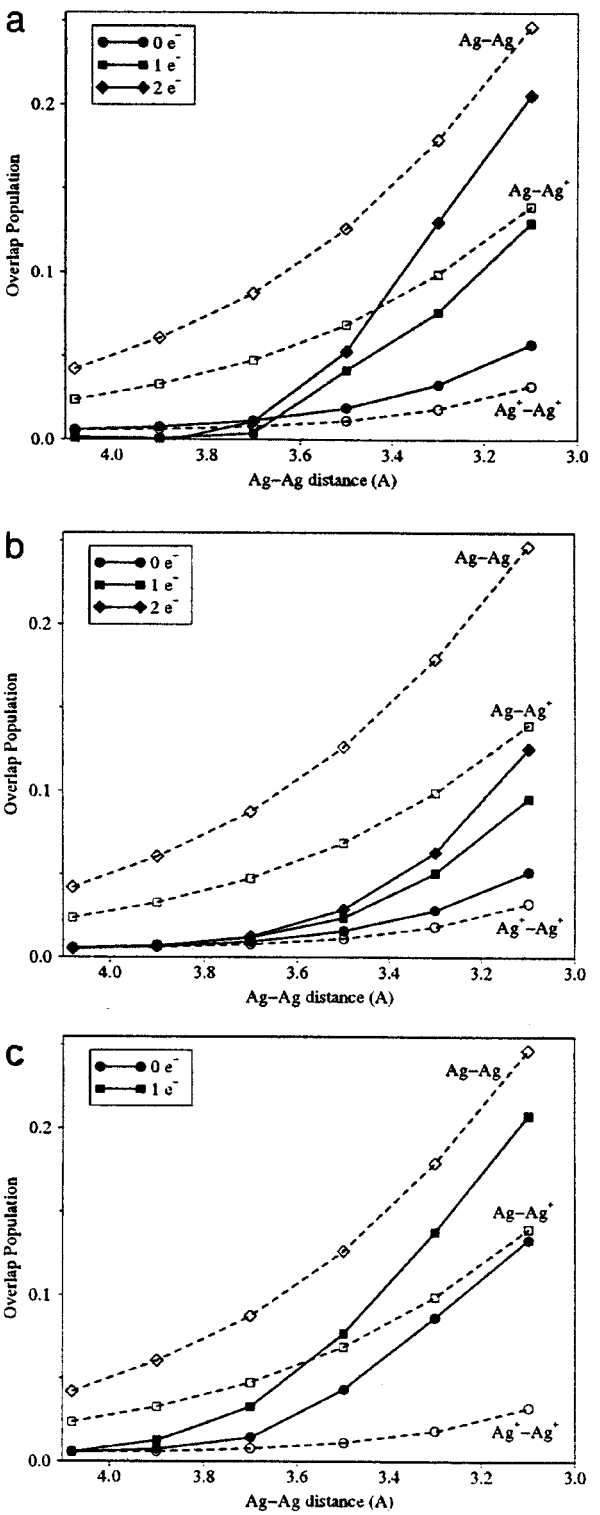

FIG. 9. The overlap population is plotted versus Ag–Ag distance in each graph. The dotted curves correspond to diatomic molecular models: two Ag, two Ag^+, or one Ag and one Ag^+ atoms interacting. Each line is appropriately labeled directly on each graph. The solid curves correspond to two Ag atoms interacting on (a) the (100) surface with kink defect, (b) the (100) surface with ledge defect, and (c) the (111) surface with interstitial Au. The various choices for electron count are indicated in the legends.

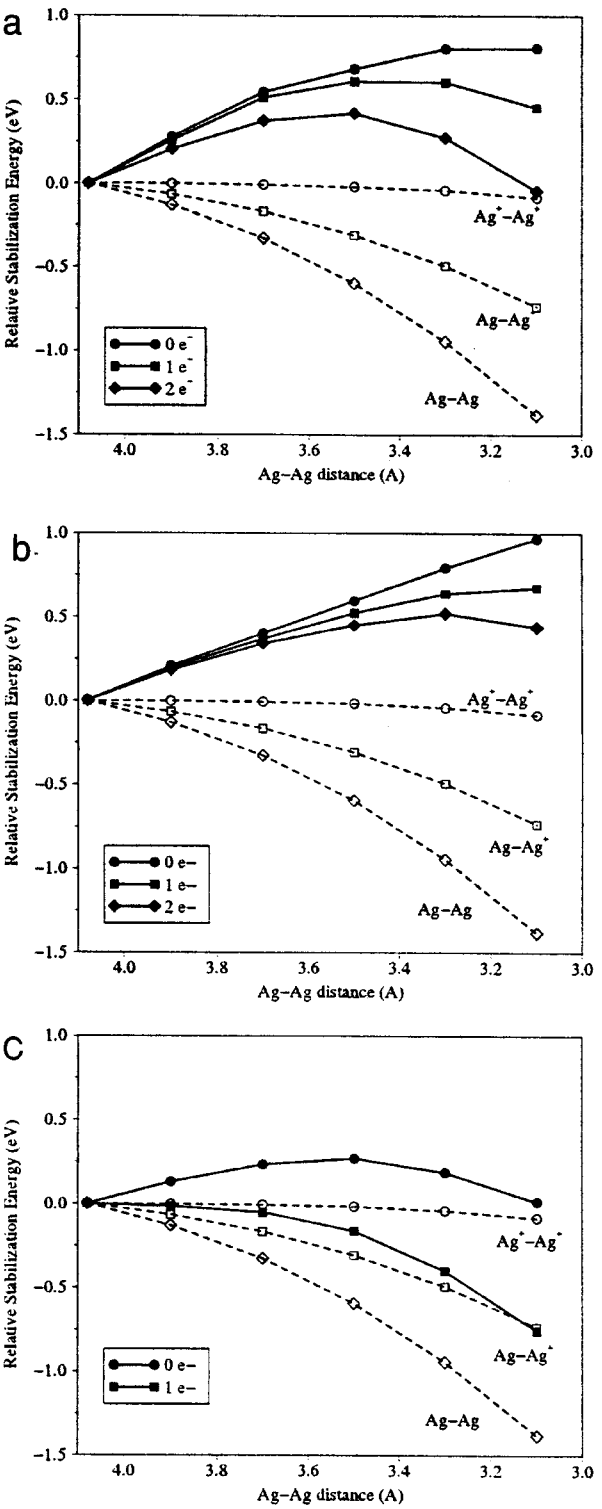

FIG. 10. The energy stabilization is plotted versus Ag–Ag distance in each graph. The dotted curves correspond to diatomic molecular models: two Ag, two Ag^+, or one Ag and one Ag^+ atoms interacting. Each line is appropriately labeled directly on each graph. The solid curves correspond to two Ag atoms interacting on (a) the (100) surface with kink defect, (b) the (100) surface with ledge defect, and (c) the (111) surface with interstitial Au. The various choices for electron count are indicated in the legends.

for the case of one electron per two Ag's than for no electron per two Ag's, though the deformation seems initially to encounter a small barrier.

Comparing the (100) and (111) surfaces, it is apparent that deformation on the latter is more favorable than on the former. For (100) surfaces, deformation at a kink defect is more favorable than at a ledge defect. There is greatest energy stabilization for one Au and one electron per two Ag's. It is clear that formation of a latent subimage cluster is more favored in a (111) surface than in a (100) surface, and the presence of an Au serves to enhance the energy stabilization of the latent subimage cluster.

The Effect of S Impurity

As was mentioned in the introduction, commercially prepared photographic film also contains sulfur in the form of Ag_2S or Ag_3AuS_2. These compounds are formed on the surface of the AgBr microcrystal and have been referred to in the photographic community as "sensitivity specks" (1). The sensitivity specks are on the order of 15 Å or less (26a) in size and it has been observed that the latent image forms preferentially at these sites on the AgBr(111) surface (26b).

Ag_2S exists in three polymorphs: one found at low temperatures and two others which are found at temperatures greater than 170°C (27). The sensitivity specks are composed of the low temperature phase, a direct band-gap semiconductor, which crystallizes in the monoclinic space group $P21/n$ (28). This compound has been extensively studied for ionic conductivity (27, 29, 30).

Recently, a high-resolution electron microscopy study was done to investigate the geometry of the interface between AgBr and Ag_2S (26a). It was found that Ag_2S will form an interface via its (100) surface[5] when grown on AgBr(111) surfaces. The Ag_2S grows epitaxially on the AgBr(111) surface[6] and has a lattice misfit of 1–2%.[7]

Figure 11 shows the structure of Ag_2S looking at the (010) face. The unit cell contains eight Ag's, which are distributed equally between two different crystallographic sites, and four S's. The two different Ag sites, represented by black and gray circles, are in either distorted tetrahedral or octahedral coordination, respectively, by the S's. The nearest Ag–S distance is 2.50 Å while the shortest S–S contact is 4.08 Å. It is interesting to note that the nearest Ag–Ag distances are 3.04 Å, suggesting that there is already some Ag–Ag bonding in this compound.

[5] The (102), (104), or (10$\bar{3}$) faces will also form interfaces with the AgBr(111) surface.

[6] The AgBr(111) surface reconstruction that was described earlier applies to a bare surface. The growth of Ag_2S specks upon this surface will change its morphology.

[7] Although a 2% mismatch is rather large, it should be kept in mind that the Ag_2S sensitivity specks are on the order of 15 Å in dimension; thus even a 2% mismatch is not unreasonable.

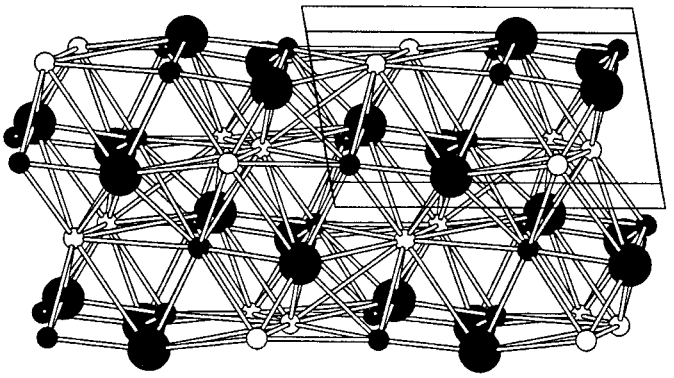

FIG. 11. The structure of monoclinic, low temperature Ag_2S. The small circles, black and gray, represent Ag in two different crystallographic positions. The large black circles are S. The unit cell of Ag_2S is outlined in the upper right hand side. The viewer is looking at the (010) face. The (100) face, which will make the interface with AgBr, is the top (and bottom) face. The close Ag–Ag distance discussed in the text is between a gray and a black Ag.

The interface between Ag_2S and AgBr is formed by the (100) surface of the former and the (111) surface of the latter. The Ag and S comprising the (100) surface can be seen in the top and bottom layers of Fig. 11. A schematic diagram of the calculational model is shown in Fig. 12. The $Ag_2S(100)$ and the AgBr(111) planes are separated by 2.33 Å.

Calculations were done on bulk Ag_2S, an $Ag_2S(100)$ slab model, an unreconstructed AgBr(111) slab model, and an $Ag_2S(100)$: AgBr(111) interface model. The Ag_2S slab model was constructed by stacking in the [100] direction three unit cells of Ag_2S. The details of the AgBr(111) slab model were given earlier. However, in this case, the topmost layer of Ag was not reconstructed; thus there are eight full layers in the model (starting with a Br layer and ending with an Ag layer).

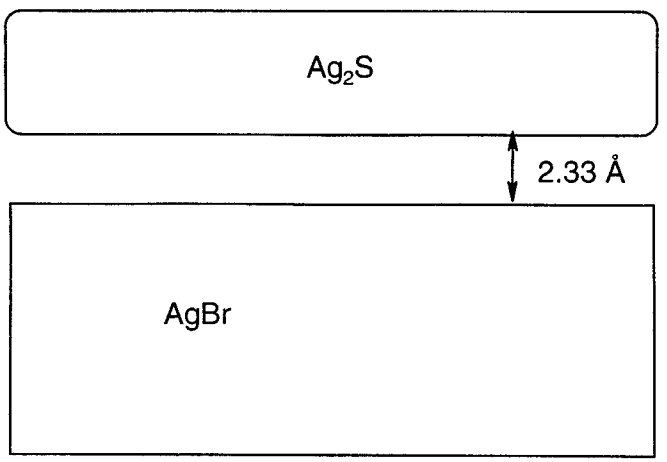

FIG. 12. A schematic view of the AgBr : Ag_2S interface. The Ag_2S is in the same orientation as in Fig. 11. In the calculational model, the Ag_2S is placed on the AgBr(111) surface at a separation of 2.33 Å.

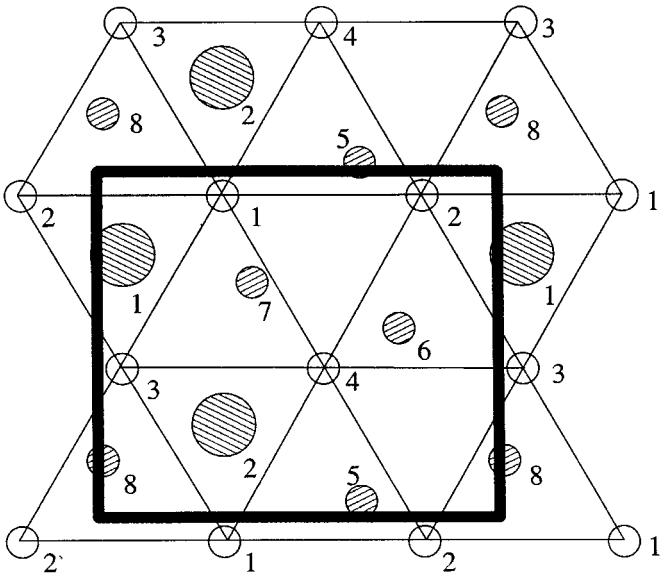

FIG. 13. The relative positions of the atoms at the interface is shown. The viewer is looking at the $Ag_2S(100)$ surface superimposed on the AgBr(111) surface. The open circles connected by a triangular grid represent the Ag of the AgBr(111) surface. The smaller shaded circles are S of Ag_2S and the large shaded circles are the Ag of Ag_2S. Please also refer to Fig. 11 to see the relative positions of the Ag and S in Ag_2S. The numbers correspond to the labels in Table 1, which lists the interatomic distances at the interface.

The interface model was constructed by placing the $Ag_2S(100)$ slab on the Ag layer of the AgBr(111) slab in positions that were suggested by the experimental results (26a) (Figs. 12 and 13). In each unit cell, the two S's of Ag_2S are each three-fold coordinated by the Ag of AgBr. The remaining four Ag of Ag_2S are found in similar three-fold coordination sites. The nearest neighbor distances of the atoms at the interface are given in Table 1. Note that some silver–silver separations are quite short (3.15 Å), which will lead to some Ag–Ag interactions at the interface.

First consider the results of the Ag_2S calculation (Fig. 14). The projected DOS is that for Ag. The calculated band gap is approximately 2.5 eV, larger than the experimentally

TABLE 1
Interatomic Distances at the Interface
(see Fig. 13 for the geometry)

	Ag1	Ag2	Ag3	Ag4
S1	4.00 Å	7.03 Å	4.00 Å	5.72 Å
S2	5.18 Å	6.63 Å	3.25 Å	3.32 Å
Ag5	7.32 Å	3.28 Å	5.97 Å	3.94 Å
Ag6	5.21 Å	4.09 Å	6.08 Å	3.16 Å
Ag7	3.42 Å	5.03 Å	4.20 Å	3.82 Å
Ag8	6.33 Å	8.77 Å	3.15 Å	5.49 Å

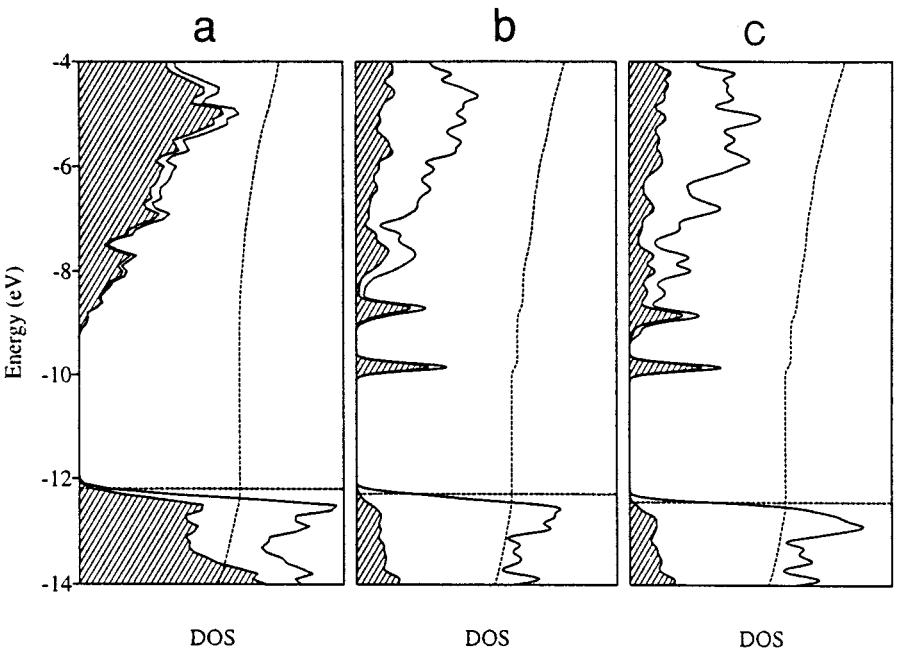

FIG. 14. The DOS of bulk and slab Ag_2S. (a) Bulk Ag_2S : Ag proj.; (b) Ag_2S slab : surface Ag; and (c) "stretched" slab surface Ag. Please refer to the text for details.

reported band gap of 1.4 eV. However, band gap measurements of Ag_2S may not be reliable because it is an ionic conductor, and experimentally reported values are not very precise.

Figure 14b shows the DOS of the $Ag_2S(100)$ slab model. Notice the peak in the DOS that appears just below the conduction band. This peak in the DOS (which is reminiscent of the AgBr(111) surface calculations presented before) arises primarily from the Ag at the $Ag_2S(100)$ surface as shown by the projected DOS. These states will change upon interaction with the AgBr surface to form the interface.

As mentioned earlier in this section, there is a lattice mismatch between the two structures. The lattice parameters for the AgBr(111) surface are slightly larger than those for the $Ag_2S(100)$ surface. Figure 13 shows the 7.07 Å × 8.17 Å unit cell of AgBr that was used in the calculations. This is slightly larger than the 6.91 Å × 7.87 Å unit cell of the $Ag_2S(100)$ face. It is necessary to "stretch" the Ag_2S lattice to "fit" the AgBr lattice because of the lattice mismatch. In the calculational model, this lattice mismatch was accommodated by increasing the unit cell dimensions of Ag_2S to match the corresponding unit cell of AgBr, before the two slabs were brought together. The positions of the atoms within the unit cell were not changed; only the unit cell dimension was increased (by 0.1 and 0.2 Å, respectively). The DOS of this "stretched" slab of Ag_2S (not shown here) is essentially the same as what is shown in Fig. 14b. This stretched slab is now ready to be brought toward the AgBr(111) surface to form the interface.

Figure 15 shows the results of the interface calculation. The leftmost DOS (Fig. 15a) shows the DOS of the AgBr(111) slab.[8] The peak at the bottom of the conduction band arises from the surface Ag, as was shown earlier. These surface states are the ones that will change upon forming the interface. The rightmost DOS (Fig. 15c) is that of the $Ag_2S(100)$ slab. Figure 15b shows the resulting DOS after interaction of the two slabs. Note that the band gap has become much smaller and that there are some peaks in the conduction band that have moved down in energy. These peaks, as shown by the projected DOS, arise primarily from Ag at the interface. This suggests that there are some states at the AgBr : Ag_2S interface that can serve as traps for photoelectrons. Also, because of the smaller calculated band gap, the energy required to produce a photoelectron is less at the AgBr : Ag_2S interface than in either bulk material, thus enhancing latent image formation. We have not, however, studied the formation of silver clusters at this interface.

CONCLUDING REMARKS

The purpose of this investigation has been to suggest a mechanism for the formation of a subimage cluster on an AgBr(100) surface, to account for the differences in

[8] As was explained before, the bare AgBr(111) surface does undergo reconstruction. The DOS of the unreconstructed surface is shown in order to probe the evolution of the DOS upon formation of the interface.

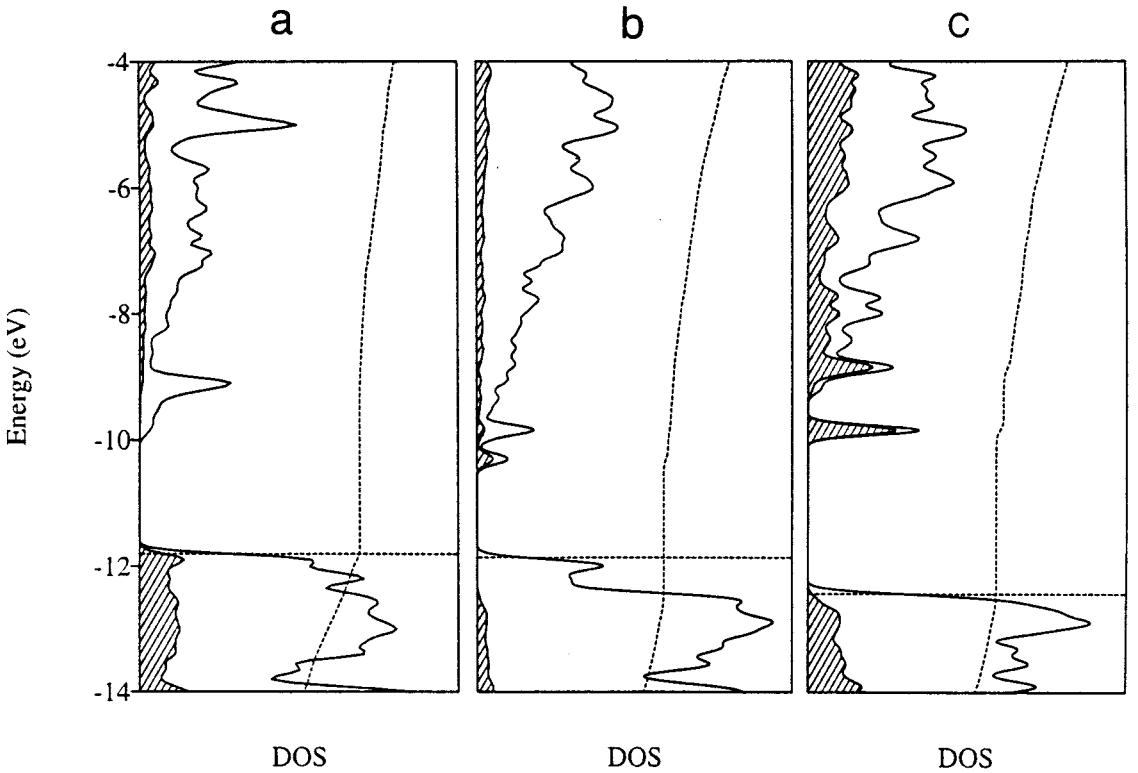

FIG. 15. (a) The DOS of an AgBr(111) slab. (b) The resulting DOS after the two slabs are brought together. (c) The DOS of an $Ag_2S(100)$ slab. The peaks at the bottom of the conduction band in the middle panel are due primarily to Ag at the interface.

photographic sensitivity displayed by the (111) and (100) surfaces, and to account for the effect of Au and S impurities in enhancement of photographic sensitivity. Previous workers had postulated the existence of "shallow trapping sites" (31) for photoelectrons on the surface of AgBr. Also, it was believed that after the trapping of a photoelectron, an Ag^+ ion would migrate to this site, followed by the capture of another photoelectron to form the Ag_2 subimage center. However, although the stability of the Ag_2 subimage center in different configurations on the surface has been studied (18), the exact nature of the trapping site and mechanism for formation of a subimage cluster were not given. In our recent publication (5), we suggested that the electronic trapping site in the case of the AgBr(111) surface is a band of levels, a reconstructed surface Ag *s*-state, which lies just below the bulk conduction band, in agreement with previous models. Population of this band by electrons induces Ag ion reduction and pair formation.

In this work, a similar band of levels was found for an AgBr(100) model with a kink defect, but not with the ledge defect. We suggest that this is one explanation for the empirical observation of the greater photographic sensitivity of a (111) surface over a (100) surface.

Our calculations show that a pairing distortion on the AgBr(100) surface with a kink defect is feasible. Deformation on a (111) surface is more favorable than on a (100) surface with a kink defect. In the ledge defect model, we suggested a plausible mechanism for distortion that could lead to formation of an Ag_2 center. However, the calculations have shown that this is the least favorable of the three distortions considered. All of these models suggest that stabilized, reduced Ag–Ag pairs form on the surface. These models provide a possible explanation for the empirical observation that the (111) surface possesses greater photographic sensitivity than the (100) surface.

Other calculations dealing with the (100) surface (16–18) have been concerned with the stability of a latent image cluster adsorbed on the surface. In agreement with our calculations, it was found (18) that a Ag_2 center is stable at a kink site, although no mechanism for its formation on the surface was suggested.

What about the effect of gold? It is commonly held that gold is incorporated in a latent image cluster and thus increases the sensitivity of AgBr to the formation of a latent image cluster. Previous investigators had postulated (19, 32) that this was due to a superior electron trapping site provided by Au. Our results do not support this hypothesis, because the DOS near the band gap remains unchanged upon inclusion of Au (please compare Figs. 8 and 2b). The effect of an Au interstitial, rather, is to transfer electrons to

the surface Ag atoms. As suggested by the model, this partial internal reduction sensitizes the surface Ag, demanding fewer photoelectrons to form a subimage center and even facilitating the formation of subimage centers in the absence of photoelectrons. This is in agreement with experimental observation that Au^0 increases fog (21).

The Au may also affect indirectly the stability of an Ag–Ag bond. Indeed, in these calculations (please see Figs. 9 and 10), the greatest energy stabilization and overlap population were found for the case of one photoelectron added to one Au interstitial. This indicates that an Au interstitial does contribute to the stability of a subimage center. Again, this observation is in agreement with experimental data which show that the presence of gold reduces the size of a stable latent image cluster that is required for developability (1, 33), thus conferring greater photographic sensitivity.

These two seemingly contradictory observations about the role of gold (fog versus sensitization) can be resolved if it is recalled that, in this computational model, gold was included as Au^0. The model shows that Au^0 will enhance formation of a subimage center even in the absence of photoelectrons (causing fog) but that once a subimage center is formed, gold confers greater stability. It is likely that if gold were introduced into a subimage center via silver gold sulfide (as Au^+), the beneficial effects of sensitization would be retained and the harmful effects of fog formation removed. Indeed, some investigators have postulated that so called "Au plus S sensitization centers" could provide better trapping sites for photoelectrons (1b).

At present, there is not enough experimental data available to allow the construction of an $AgBr:Ag_3AuS_2$ interface model in order to probe this hypothesis. However, our calculations with Ag_2S suggest that this is plausible. The computations reveal some states at the interface that can serve as shallow traps for photoelectrons. Furthermore, the band gap, upon formation of the interface, is diminished, which suggests that it requires less energy to produce photoelectrons at the interface. This finding supports the empirical observations that greater photographic sensitivity is achieved by the incorporation of Ag_2S on the surface of AgBr.

APPENDIX

All calculations were done using the extended Hückel method, a semi-empirical molecular orbital method (34) with the program YAeHMOP by Greg Landrum. The parameters are given in Table 2. The unit cells used in the two-dimensional calculations are outlined in Figs. 1, 3, 5, and 13 by heavy lines. The unit cell for the AgBr(111) with Au model consisted of 34 atoms and for the AgBr(100) models consisted of 88 atoms.

DOS and band structure calculations of bulk (3-dimensional) AgBr were done with a primitive unit cell and were compared with previous calculations (35–37) done using other techniques. The extended Hückel calculations on bulk AgBr reproduced the earlier results.

TABLE 2
Extended Hückel Parameters Used

Atom	Orbital	H_{ii}	ζ_1	ζ_2	C_1	C_2
Ag	5s	−10.5	2.244			
	5p	−5.8	2.202			
	4d	−14.5	6.07	2.663	0.5591	0.6048
Br	4s	−22.07	2.588			
	4p	−13.1	2.131			
S	3s	−20.00	1.817			
	3p	−13.30	1.817			

The relative energy stabilization was calculated by subtracting the total energy of the undistorted model from the total energy of the distorted model (after pairwise distortion of the two surface Ag) in each case. Thus, a positive value meant a destabilization, while a negative value meant a favorable distortion.

The "slab" model for the surface was chosen after doing calculations on a series of models having from 5 to 12 layers. In each model, the DOS and the average net charges on the atoms in the innermost layers were compared with values obtained from the calculation on bulk AgBr. It was found that 7 layers for AgBr(111) and 5 layers for AgBr(100) were sufficient to model bulk properties in the innermost layer.

ACKNOWLEDGMENTS

We are grateful to Imation Corporation for its support of our research, in a productive academic and industrial collaboration.

REFERENCES

1. T. Tani, "Photographic Sensitivity: Theory and Mechanisms", (a) p. 81, (b) p. 165. Oxford University Press, New York, 1995.
2. D. A. Pitt, M. L. Rachu, and M. R. V. Sahyun, *Phot. Sci. Eng.* **25,** 57 (1981).
3. (a) S. H. Ehrlich, *Phot. Sci. Eng.* **23,** 348 (1979). (b) P. Faelens, *J. Phot. Sci.* **26,** 144 (1978).
4. H. E. Spencer, *J. Imaging Sci.* **32,** 28 (1988).
5. A.-S. Malik, F. J. DiSalvo, R. Hoffmann, and J. T. Blair, *J. Imaging Sci. Tech.* **42,** 210 (1998).
6. R. Hoffmann, "Solids and Surfaces: A Chemist's View of Bonding in Extended Structures," (a) p. 36, (b) p. 42, (c) p. 62, (d) p. 92. VCH, New York, 1988.
7. R. W. Gurney and N. F. Mott, *Proc. Roy. Soc. London, Ser. A* **164**, 151 (1938).
8. H. Haefke and M. Krohn, *Surf. Sci. Lett.* **261,** L39 (1992).
9. G. Hegenbart and T. Muüssig, *Surf. Sci. Lett.* **275,** L655 (1992).
10. H. Hofmeister, S. Grosse, G. Gerth, and H. Haefke, *Phys. Rev. B.* **49,** 7646 (1994).
11. R. C. Baetzold, Y. T. Tan, and P. W. Tasker, *Surf. Sci.* **195,** 579 (1988).
12. Y. T. Tan, K. J. Lushington, P. Tangyunyong, and T. N. Rhodin, *J. Imaging Sci. Tech.* **36,** 118 (1992).

13. P. Tangyunyong, T. N. Rhodin, Y. T. Tan, and K. J. Lushington, *Surf. Sci.* **255,** 259 (1991).
14. F. C. Brown, *J. Phys. Chem.* **66,** 2368 (1962).
15. L. E. Brady and J. F. Hamilton, *J. Appl. Phys.* **37,** 2268 (1966).
16. R. C. Baetzold, *Phot. Sci. Eng.* **19,** 11 (1975).
17. (a) J. Flad, H. Stoll, and H. Preuss, *Z. Phys. D* **6,** 287 (1987). (b) J. Flad, H. Stoll, A. Nicklass, and H. Preuss, *Z. Phys. D* **15,** 79 (1990).
18. R. C. Baetzold, *J. Phys. Chem. B* **101,** 8180 (1997).
19. F. W. H. Mueller, *J. Opt. Soc. Am.* **39,** 494 (1949).
20. J. Bourdon and A. Bonneret, *Sci. Ind. Photogr.* **32** (1961).
21. E. Moisar, *Phot. Sci. Eng.* **25,** 45 (1981).
22. P. Tangyunyong, T. N. Rhodin, Y. T. Tan, and K. J. Lushington, "Gold Adsorption on AgBr(111) and (100) Surfaces: SEXAFS Study of Surface Structure and Bonding," unpublished.
23. K. M. Merz Jr. and R. Hoffmann, *Inorg. Chem.* **27,** 2120 (1988).
24. P. K. Mehrotra and R. Hoffmann, *Inorg. Chem.* **17,** 2187 (1977).
25. P. Pyykkö, *Chem. Rev.* **97,** 597 (1997).
26. (a) T. Shiosawa and T. Kobayashi, *Phys. Stat. Sol.* **110,** 375 (1988). (b) J. W. Mitchell, *J. Imaging Sci. Tech.* **42,** 215 (1998).
27. R. J. Cava, F. Reidinger, and B. J. Wuensch, *J. Solid State Chem.* **31,** 69 (1980).
28. A. J. Frueh Jr., *Z. für Kristallogr.* **110,** 136 (1958).
29. B. H. Grier, S. M. Shapiro, and R. J. Cava, *Phys. Rev. B* **29,** 3810 (1984).
30. R. J. Cava and D. B. McWhan, *Phys. Rev. Lett.* **45,** 2046 (1980).
31. A. P. Marchetti and R. S. Eachus, "The Photochemistry and Photophysics of the Silver Halides, p. 145, Wiley, New York, 1992.
32. J. F. Hamilton, *Adv. Phys.* **37,** 359 (1988).
33. M. R. V. Sahyun, *Phot. Sci. Eng.* **27,** 171 (1983).
34. R. Hoffmann, *J. Chem. Phys.* **39,** 1397 (1963).
35. B. N. Onwuagba, *Solid State Commun.* **97,** 267 (1996).
36. (a) A. B. Gordienko, Y. N. Zhuravlev and A. S. Poplavnoi, *Phys. Stat. Sol.* **168,** 149 (1991).
37. A. B. Kunz, *Phys. Rev. B* **26,** 2070 (1982).